Symmetric Baroclinic Instability of a Hadley Cell

BASIL N. ANTAR

The University of Tennessee Space Institute, Tullahoma 37388

WILLIAM W. FOWLIS

Space Sciences Laboratory, NASA, Marshall Space Flight Center, AL 35812

(Manuscript received 8 December 1981, in final form 17 February 1982)

ABSTRACT

A stability analysis of a thin horizontal rotating fluid layer which is subjected to arbitrary horizontal and vertical temperature gradients is presented. The basic state is a nonlinear Hadley cell which contains both Ekman and thermal boundary layers; it is given in closed form. The stability analysis is based on the linearized Navier-Stokes equations, and zonally symmetric perturbations in the form of waves propagating in the meridional direction are considered. Numerical methods were used for the stability problem. The objective of this investigation was to extend previous work on symmetric baroclinic instability with a more realistic model. Hence, the study deals with flows for which the Richardson number (based on temperature and flow gradients at mid-depth) is of order unity and less. The computations cover ranges of Prandtl number $0.2 \leqslant \sigma \leqslant 5$, Rossby number $10^{-2} \leqslant \epsilon \leqslant 10^{2}$ and Ekman number $10^{-4} \leqslant E \leqslant 10^{-1}$. It was found, in agreement with previous work, that the instability sets in when the Richardson number is close to unity and that the critical Richardson number is a non-monotonic function of the Prandtl number. Further, it was found that the critical Richardson number decreases with increasing Ekman number until a critical value of the Ekman number is reached beyond which the fluid is stable. The principal of exchange of stability was not assumed and growth rates were calculated. A wavelength of maximum growth rate was found. For our model overstability was not found. Some computations were performed for Richardson numbers less than zero. No discontinuities in growth rates are noticeable when the Richardson number changes sign. This result indicates a smooth transition from symmetric baroclinic instability to a convective instability.

1. Introduction

It is well known that statically stable baroclinic flow can be destablished by two different mechanisms. The first occurs in what is usually known as ordinary baroclinic instability in which the perturbations of maximum growth rate have a wavelength in the zonal direction and the gravest possible structure in the meridional direction (Charney, 1947; Eady, 1949). This instability is well understood and has been observed experimentally (Hide and Mason, 1975). The second occurs in what is known as symmetric baroclinic instability. In this case, the instability mechanism is such that the perturbations of maximum growth rate have meridional structure but no zonal structure. This study is concerned with the latter form of instability.

Two of the earliest analyses of symmetric baroclinic instability are those of Solberg (1936) and Kuo (1956). However, the first definitive work is that of Stone. In a sequence of papers, Stone (1966, 1970, 1971) examined the stability of a parallel baroclinic flow with respect to infinitesimal, three-dimensional perturbations. Constant vertical shear and constant temperature gradients were assumed and thermal and viscous diffusion effects were neglected. Stone found that when the Richardson number Ri is between 0.95 and 0.25, waves whose axes are in the zonal direction have the maximum growth rates. Stone *et al.* (1969) and Hadlock *et al.* (1972) attempted to observe symmetric baroclinic instability in the laboratory, and some evidence of the predicted meridional structure was seen but a comprehensive experimental study of this instability has yet to be performed.

McIntyre (1970) performed an analysis of symmetric baroclinic instability which included both vertical and horizontal shears and allowed for the Prandtl number σ. The model considered was infinite in both the horizontal and vertical directions. McIntyre found, in the absence of horizontal shear, that the maximum value of Ri at which symmetric instability sets in (the critical Richardson number Ri_c) is a function of σ and can be larger than 0.95. McIntyre also found that the most unstable wavelength is infinite and that both monotonic and oscillatory instability can occur. In a related analysis, Walton (1975) considered only vertical shear in a

0022-4928/82/061280-10$06.50

finite depth fluid. When weak viscous effects are included, Walton found that Ri_c is lower for both the monotonic and oscillatory instabilities. He also found that the most rapidly growing modes display a weak functional dependence on the diffusion coefficients when those are asymptotically small.

Recently, Emanuel (1979) presented a detailed study of the linear stability of symmetric perturbations in a baroclinic flow with both horizontal and vertical shears. Retaining both the viscous and thermal diffusivities for a vertically bounded flow, Emanuel studied (i) hydrostatic disturbances and (ii) nonhydrostatic disturbances in a neutrally stratified fluid. He found that for both cases the critical Richardson number depended on both the thermal and the viscous diffusivities. He also established the fact that the most unstable normal mode is determined primarily by the depth of the unstable domain and the slope of the isentropic surfaces rather than by the diffusive properties of the fluid. Weber (1980), in a somewhat similar analysis, examined the symmetric instability of a basic state with a constant vertical shear in the presence of horizontal boundaries while taking full account of the viscous effects for arbitrary vertical (stable) stratification. Although, he made the simplifying assumption of replacing the vertical viscous and diffusive terms in the perturbation equations by a wave mode, his results compare favorably with those of Emanuel. It should be noted that in both of the above studies the analyses were restrictive; Emanuel investigated only neutral modes by invoking the principal of exchange of stability and Weber used an approximate solution to the perturbation equations. Emanuel's paper contains an excellent survey of previous work on this problem.

Previous workers have postulated symmetric baroclinic instability as the cause of certain physical phenomena. Stone (1967) conjectured that the banded structure of Jupiter's atmosphere is due to this instability. Bennets and Hoskins (1979) attributed the origin of rainbands and squall lines to this instability. Weber (1980) suggested that the generation of roll vortices in the oceans and the atmosphere is due to symmetric baroclinic instability.

In all of the theoretical studies cited above, the basic state whose stability was investigated was a postulated state in which both the shears and the temperature gradients in the vertical and the horizontal directions were taken to be constants throughout the fluid. In an experimental apparatus whose upper and lower boundaries are stationary, such a basic state is a good approximation in the interior of the fluid only; it is not a good approximation near the boundaries, especially when the Ekman number is not vanishingly small. In the study presented in this paper a fluid contained between two horizontal plates of infinite extent is considered and the influence of the Ekman and the thermal layers on symmetric baroclinic instability is investigated. The analysis uses a realistic basic state which is obtained through the solution of the governing nonlinear equations of motion for arbitrary external forcings, e.g., the Ekman number, the vertical stratification, etc. This basic state was used in a recent paper by the authors in an investigation of ordinary baroclinic instability (see Antar and Fowlis, 1981).

It is obvious that if a direct analog of a laboratory experiment is required, then this model is not sufficient since it does not allow for the side walls and the side layers. In a recent study Quon (1980, 1981) simulated laboratory conditions for the onset of symmetric baroclinic instability through the numerical solution of the full Navier-Stokes-energy equations for the flow in a cylindrical differentially heated, rotating annulus. Although such an analysis is of great value in modeling the true experimental conditions, the amount of computer time required for the calculation of each case precludes a thorough probing of the parameter space for the criteria for the onset of the instability. It is our opinion that the present study fills a needed gap between the constant-shear, constant-temperature gradient analyses discussed earlier and that of the exact solution of Quon.

The basic state model is reviewed in Section 2. The perturbation equations for the symmetric instability and their method of solution are presented in Section 3. In Section 4 we discuss the results of the present analysis and how they compare with the previous work. Our conclusions are presented in Section 5.

2. The basic state

The basic state used in the present stability analysis is identical to that used in the work of Antar and Fowlis (1981; hereinafter referred to as I). This model is described only briefly here; for further details and justifications, the reader is referred to I. We consider a Boussinesq fluid confined between two horizontal plates which are set a distance d apart. The coordinate system used is rectangular Cartesian with axes (x, y, z) corresponding to the eastward, northward and vertical directions, respectively, and with the origin midway between the plates. A sketch of the model is shown in Fig. 1. The plates are assumed to extend to infinity in the x-direction and to large distances in the y-direction. The plates and the fluid are taken to rotate as a whole about the vertical axis with a constant angular velocity Ω. A temperature gradient in which the temperature decreases linearly in the y-direction is maintained on both plates. To assure that the vertical stratification, and hence the Richardson number, is arbitrary and externally fixed, the temperatures of the upper and lower plates are set to differ uniformly by a constant amount ΔT for all (x, y).

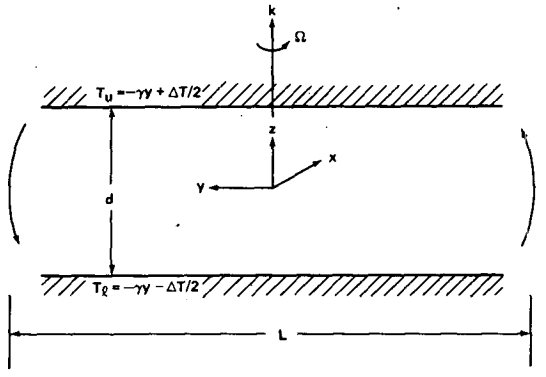

FIG. 1. A sketch of the geometry of the model and the coordinate system.

The velocity and temperature fields are governed by the Navier-Stokes, energy and mass conservation equations. Under the conditions assumed here for the basic, two-dimensional steady state, these equations, in a rotating reference frame, reduce to

$$-2V = \mathrm{E}\partial^2 U/\partial z^2, \tag{1}$$

$$2U = \mathrm{E}\partial^2 V/\partial z^2 - \partial p/\partial y, \tag{2}$$

$$V\partial T/\partial y = (\mathrm{E}/\sigma\epsilon)\partial^2 T/\partial z^2, \tag{3}$$

$$T = \partial p/\partial z, \tag{4}$$

where $\mathbf{V}$ is the velocity vector (U, V), p the pressure, T the temperature and

$$\left.\begin{aligned} \epsilon &= \alpha g\gamma/\Omega^2 \\ \mathrm{E} &= \nu/\Omega d^2 \\ \sigma &= \nu/\kappa \end{aligned}\right\}$$

are a thermal Rossby number, the Ekman number and the Prandtl number, respectively. In Eqs. (1)–(4), length, time, velocity and temperature have been made dimensionless using d, Ω^{-1}, $\alpha g d\gamma/\Omega$, and γd, where α is the coefficient of thermal expansion, γ the imposed horizontal temperature gradient and g gravity. The main assumptions used in arriving at Eqs. (1)–(4) are that the vertical velocity component W is negligible and that $\partial T/\partial y = -1$ throughout the region of interest (see I).

The solution of the system (1)–(4) which is consistent with the no slip and perfectly conducting conditions at the solid boundaries, i.e.,

$$\left.\begin{aligned} U = V &= 0 \\ T &= \pm(\Delta T/2) - y \quad \text{at} \quad z = \pm 1/2 \end{aligned}\right\} \tag{5}$$

is given by

$$U(z) = -f(z)/8 + z/2, \tag{6}$$

$$V(z) = g(z)/8, \tag{7}$$

$$T(y, z) = -y + z\Delta T + \epsilon\sigma[2z - f(z)]/8, \tag{8}$$

where

$$f(z) = [\cosh R(z + 1/2)\cos R(z - 1/2) - \cosh R(z - 1/2)\cos R(z + 1/2)]/h(R),$$

$$g(z) = [\sinh R(z + 1/2)\sin R(z - 1/2) - \sinh R(z - 1/2)\sin R(z + 1/2)]/h(R),$$

$$h(R) = \sinh^2(R/2) + \sin^2(R/2),$$

$$R = \mathrm{E}^{-1/2}.$$

The velocity and temperature profiles given by (6)–(8) are shown in Fig. 2 for different values E, ϵ, σ and ΔT. The limits of applicability of this model are discussed in I.

3. The perturbation equations

The instability problem is tackled by imposing perturbations on the basic state presented above. Since we are concerned with symmetric perturbations, the perturbation functions will be proportional to $\exp[il(y - ct)]$ which represents a wave with meridional wavenumber l propagating in the meridional direction with speed c. Introducing the perturbations into the Navier-Stokes, energy and mass conservation equations and upon linearizing the perturbation equations we obtain the following equations for the perturbation functions:

$$\mathrm{E}(D^2 - l^2)^2 w + il[(c - \epsilon V)(D^2 - l^2)w + \epsilon w D^2 V] + 2ilDu - l^2\theta = 0, \tag{9}$$

$$\mathrm{E}(D^2 - l^2)u + il(c - \epsilon V)u - \epsilon w DU + 2il^{-1}Dw = 0, \tag{10}$$

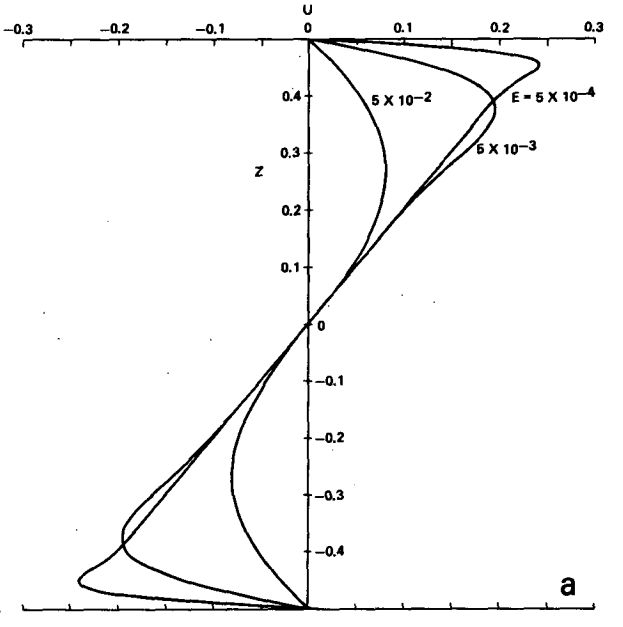

FIG. 2a. The zonal velocity component U of the basic state as a function of z, for three values of E.

$$E(D^2 - l^2)\theta + il\sigma(c - \epsilon V)\theta + i\epsilon l^{-1}\sigma Dw - \epsilon\sigma wDT = 0, \quad (11)$$

$$ilv + Dw = 0, \quad (12)$$

where

$$D = d/dz.$$

In the above the perturbation velocity is $\mathbf{v} = (u, v, w)$ and θ is the perturbation temperature. Note that the perturbation equations are not hydrostatic.

To complete the specification of the problem, the following boundary conditions are imposed on the perturbation functions:

$$u = w = Dw = \theta = 0 \quad \text{at} \quad z = \pm 1/2. \quad (13)$$

The perturbation problem as posed constitutes an eigenvalue problem. We take l to be real and $c = c_r + ic_i$ to be complex, where c_r denotes the propagation speed and c_i, the growth rate. Monotonic instability occurs for $c_i \geqslant 0$ while $c_r = 0$, whereas overstability occurs for $c_i = 0$ while $c_r \neq 0$. It is tempting at this stage to invoke the principle of exchange of stability and to set $c_r = c_i = 0$ and hence look for neutral modes alone and reduce the number of parameters involved. Emanuel (1979) adopted this procedure. However, since McIntyre (1970) had established that for his model (see Section 1) oscillatory instability exists, it was decided to leave c_r and c_i as eigenvalues of the problem. Using this method the analysis will allow us to compute growth rates and to determine if overstability exists.

The solution to the problem (9)–(13) is obtained through numerical integration of the full eighth-order differential system. This procedure was necessary because the coefficients in the equations (i.e., the basic state) are functions of the height z. If we wish to account fully for the Ekman and thermal layers, the solution cannot be obtained in a closed form. Note that if the basic state profiles had been taken to be linear in z, as was done in most of the previous work on the symmetric baroclinic instability problem, then the set of governing equations would reduce to a differential system with constant coefficients whose solution could be determined in a closed form.

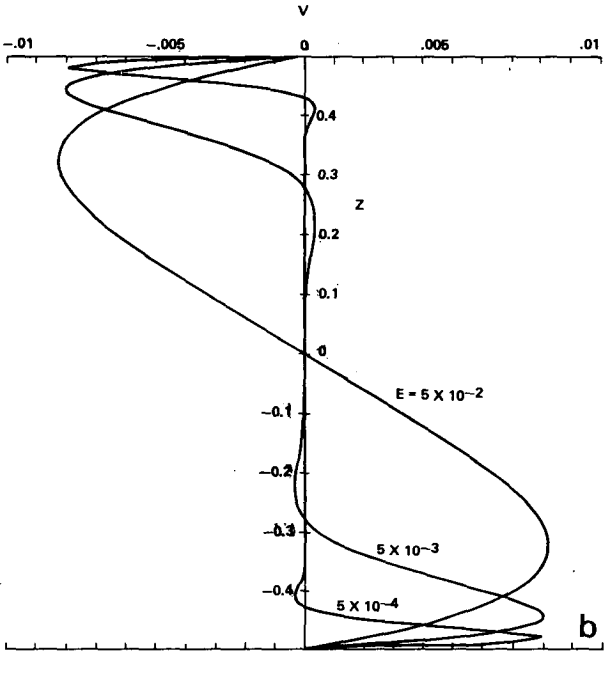

FIG. 2b. As in Fig. 2a except for the meridional component V.

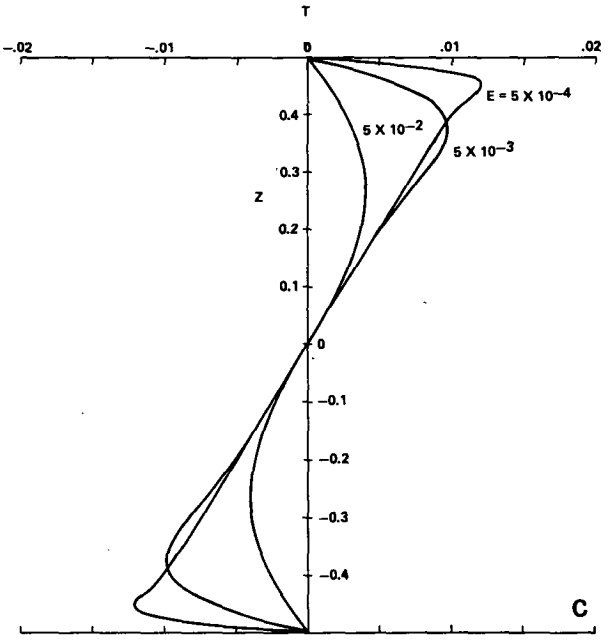

FIG. 2c. Basic state temperature profiles T at $y = 0$ for the same values of E as the results shown in Fig. 2a and for $\sigma = 1$, $\epsilon = 1$ and $\Delta T = 0$.

The numerical solution was obtained using the shooting technique. The code was identical to the one used in I, and more details of the numerical work are given in I. Briefly, the shooting technique was enhanced with the orthonormalization method, allowing the stability analysis to be performed even when the Ekman number is very small. A Newton-Raphson method was implemented for convergence on the eigenvalues, and an eighth-order Runge-Kutta method was used for the integration of the initial value problem.

4. Results and discussion

The results which follow constitute the solution of the eigenvalue problem posed by (9)–(11) with the boundary conditions (13) for prescribed values of the parameters. The parameters of the problem which appear explicitly in the equations are ϵ the thermal Rossby number, E the Ekman number, σ the Prandtl number, ΔT the imposed vertical temperature dif-

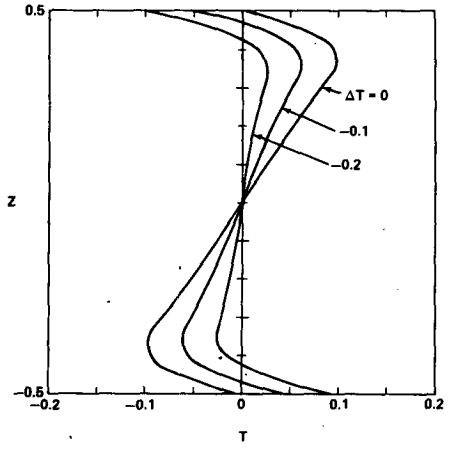

FIG. 3. Basic state temperature profiles T at $y = 0$ for three values of ΔT and for $\sigma = 1$, $\epsilon = 1$, and $E = 5 \times 10^{-3}$.

ference, and l and c the wavenumber and wave speed, respectively. Note that the first four parameters appear in the basic state as well as the perturbation equations, but the last two belong to the stability problem alone.

As was discussed in Section 1, the Richardson number plays a significant role in the symmetric baroclinic instability problem. While this number does not appear explicitly in our formulation of the basic state, it may be defined using the parameters which do appear explicitly. The Richardson number is defined by

$$\mathrm{Ri} = \frac{\alpha g \partial T^*/\partial z^*}{(\partial U^*/\partial z^*)^2}, \tag{14}$$

where $\partial T^*/\partial z^*$ and $\partial U^*/\partial z^*$ are the dimensional basic state temperature and zonal flow gradients, respectively. It is obvious from this definition and from expressions (6)–(8) that for the present model Ri is not a constant but is a function of z. We may define a "bulk" Richardson number by the value of Ri at mid-depth between the horizontal plates, *viz*,

$$\mathrm{Ri}_b = \alpha g \left.\frac{\partial T^*/\partial z^*}{(\partial U^*/\partial z^*)^2}\right|_{z=0}.$$

In all of the subsequent discussion, Ri_b will be used instead of Ri and the subscript b will be dropped. We shall see that this definition is not only convenient, but it has dynamical significance in this problem. Substituting the temperature and velocity gradients for the basic state [expressions (6) and (8), respectively] into the above definition, we obtain

$$\mathrm{Ri} = 4\epsilon^{-1}(\Delta T + \tfrac{1}{4}\sigma\epsilon), \tag{15}$$

which is a constant and defined exclusively by the basic state.

The above definition shows that Ri is a function of the explicit parameters of the problem. This relationship was used when choosing values of ϵ, ΔT and σ for each eigenvalue search in order to be sure that we were within the correct range of Ri for instability. Stone (1970) and McIntyre (1970) showed that symmetric baroclinic instability occurs for Ri close to unity (see Section 1). The above definition indicates that for a given value of σ, there is a range of ϵ and of ΔT for which the critical value of Ri is achieved.

For $\sigma = 1$, expression (15) specifies that ΔT must be less than zero to obtain the desired range of values of Ri for instability regardless of the value of ϵ. However, setting $\Delta T < 0$ arbitrarily could lead to an unstable vertical stratification in the interior and hence a negative value of Ri. Instabilities occurring under the above conditions with negative Ri are not classed as symmetric baroclinic instabilities and are outside the range of interest of this paper. Such instabilities have been discussed by Hathaway *et al.* (1979, 1980). To obtain symmetric baroclinic instability for $\sigma = 1$, ΔT must be set negative with the additional constraint of $|4\Delta T/\epsilon| < 1$. Clearly, there exists a range of values ΔT which satisfies these two criteria. We decided to proceed with $\Delta T = -0.2$ for $\sigma = 1$. Fig. 3 shows that this value of ΔT keeps the interior vertical stratification stable. The above arguments reveal that the correct choice of ΔT for symmetric instability is a delicate matter and depends strongly on σ. Expression (15) should be of great value in guiding experimental searches for symmetric baroclinic instability in the laboratory.

Fig. 4 shows the growth rates for different values of the meridional wavenumber l as a function of ϵ for $E = 10^{-3}$, $\Delta T = -0.2$ and $\sigma = 1$. Note the existence of unstable modes over a finite range of ϵ. This feature resembles the growth rate properties of

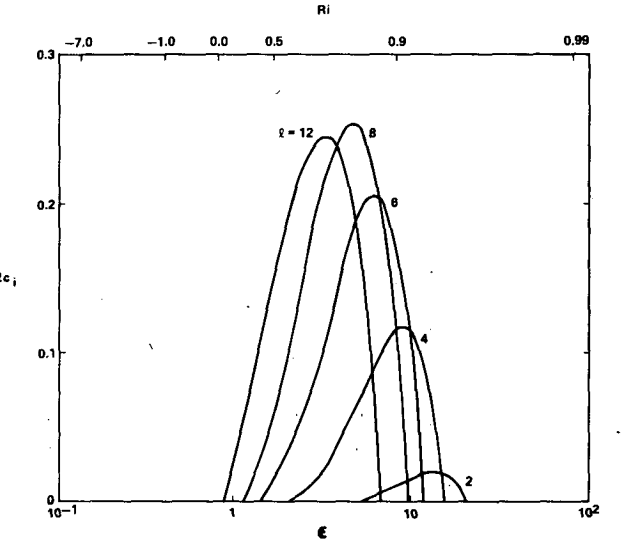

FIG. 4. Growth rates lc_i as a function of ϵ for different values of l and for $\sigma = 1$, $\Delta T = -0.2$ and $E = 10^{-3}$. The upper abscissa shows the values of Ri corresponding to ϵ.

ordinary baroclinic instability. The unstable region in ϵ is bounded by two stable regions, one in which Ri is close to unity and the other in which Ri is small or negative (Ri = $1 - 0.8/\epsilon$).

Fig. 4 also shows that as ϵ varies, the growth rate has a maximum value for a specific value of the wavenumber. Fig. 5, which is for the same values of the parameters as the results in Fig. 4, is a plot of the maximum growth rate for each wavenumber versus wavenumber. The greatest growth rate occurs for about $l = 10$. This result is at variance with the findings of Stone (1970), who found that the maximum growth rate is achieved as $l \rightarrow \infty$, and McIntyre (1970), who found that it is achieved as $l = 0$. However, since both of these previous studies are for idealized basic states, it is concluded that including the viscous effects through the Ekman and thermal layers determines the wavelength of maximum growth rate for the symmetric baroclinic instability problem.

Fig. 6, which is for the same values of the parameters as the results in Figs. 4 and 5, shows neutral stability curves in the (E-ϵ) number plane for three different wavenumbers. A significant feature of these curves is the existence of the maximum (critical) value of E above which all modes are stable. Another feature is the existence of two stable regions, or two branches of the neutral stability curves, for all values of E smaller than the mode critical values. Note that these curves are loci of points for which $c_i = 0$. For all the modes shown in this figure and those in the previous and subsequent figures, the value of the wave speed c_r was always found to be zero, indicating that these are monotonic instability modes and that the principle of exchange of stability holds for this problem. Throughout this work we did not find any oscillatory unstable modes. Thus, it is doubtful if overstability exists for the present problem.

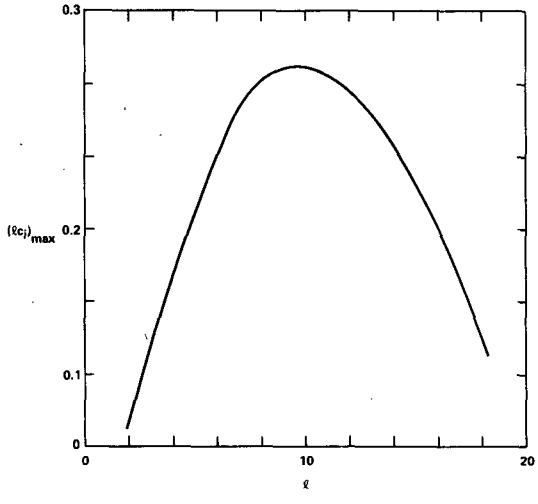

FIG. 5. The maximum growth rates as a function of the meridional wavenumber l, for the same conditions as Fig. 4.

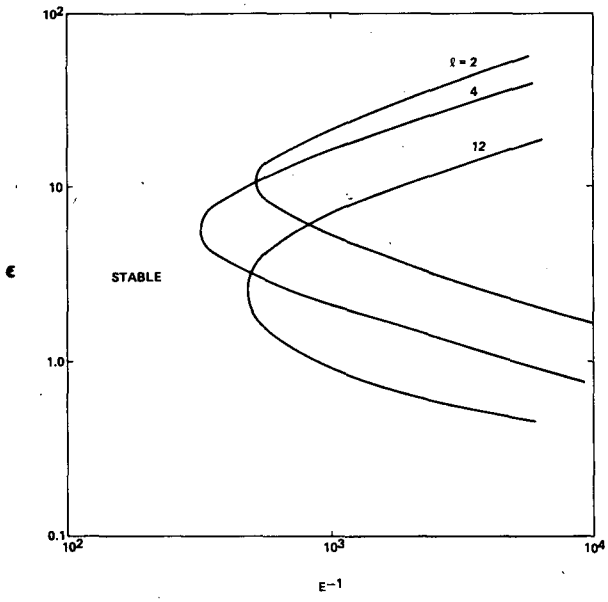

FIG. 6. Neutral stability curves, $c_i = 0$, as functions of E and ϵ for different values of l and for $\sigma = 1$ and $\Delta T = -0.2$.

The curves in the upper portion of Fig. 6 indicate that $\epsilon \rightarrow \infty$ as $E \rightarrow 0$ for all of the wavenumbers shown. To observe this criterion in terms of Ri, the neutral curves of Fig. 6 are plotted again in the (E-Ri) plane in Fig. 7. Fig. 7 shows that as $E \rightarrow 0$, the upper branches of the curves approach Ri = 1 for all wavelengths and that the region of instability increases with increasing wavenumber. Weber (1980), in his model for symmetric baroclinic instability (see Section 1), found the critical value of Ri, Ri_c, to be a monotonically decreasing function of E as the latter increases from zero. The results in Fig. 7 show that this fundamental dependence is correct up to the value of E_c, but above that value there is a region of absolute stability regardless of the value of Ri. We believe that the existence of E_c is due to the accurate inclusion of the viscous and thermal diffusive effects in our model. None of the previous work included both of these effects properly.

To investigate the effects of the Prandtl number on the stability criteria discussed above, we proceeded to find solutions for $\sigma = 5$. As was discussed earlier, changing the value of σ necessitates a search for the appropriate value of the vertical temperature difference ΔT such that Ri is in the proper range for symmetric baroclinic instability. The value chosen for $\sigma = 5$ was $\Delta T = -4.5$, which allows Ri to be in the vicinity of unity (Ri = $5 - 18/\epsilon$). Fig. 8 shows the growth rates as a function of ϵ for the above values of σ and ΔT and for $E = 10^{-3}$. Again, it is seen that the unstable modes separate two stables regions in ϵ (or Ri). Fig. 8 shows that the maximum growth rate increases with increasing wavenumber l. In fact, the total range of instability increases with

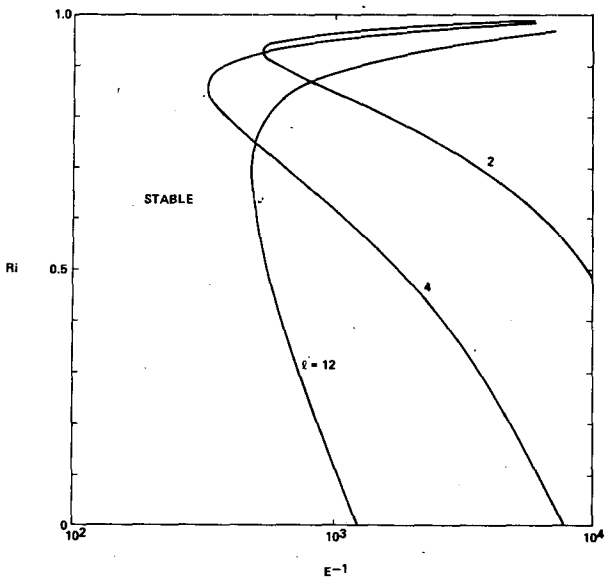

FIG. 7. The neutral stability curves of Fig. 6 as functions of E and Ri.

l. Note that the upper bound of instability in ϵ first increases with increasing wavenumbers up to $l = 4$ and then decreases, reaching an asymptotic value of $\epsilon = 4.55$ for $l \geqslant 6$ which corresponds to Ri = 1 for the parameters used. Another feature, which is different from the $\sigma = 1$ case, is that the maximum growth rates occur for approximately the same value of ϵ for all the wavenumbers shown. For this case this value of ϵ translates to a value of Ri = −4!

Fig. 9, which is for the same values of the parameters as the results in Fig. 8, shows the variation of the maximum growth rates as a function of the wavenumber l. This figure reveals that there is still a wavenumber of greatest growth rate which occurs about $l = 13.5$. However, the decrease in the growth rate is much smaller for wavenumbers above the maximum value than it is for the $\sigma = 1$ results (see Fig. 5).

The neutral stability curves in the (E-Ri) plane are shown in Fig. 10 for $l = 1$ and 4. In this figure only the positive part of the Ri range is shown. Note that there are two values of Ri_c as $\mathrm{E} \rightarrow 0$, each corresponding to one wavenumber, and that the range of instability is much larger for $l = 4$ than that for $l = 1$.

To appreciate more fully the influence of the Prandtl number on the symmetric instability criteria, Fig. 11 which shows the neutral stability curves for $l = 4$ in the (E-Ri) plane for $\sigma = 1$ ($\Delta T = -0.2$), $\sigma = 2$ ($\Delta T = -1.5$) and $\sigma = 5$ ($\Delta T = -4.5$) was prepared. Except for $\sigma = 1$, only the upper branches of the curves appear for Ri > 0. All the curves shown tend to specific asymptotic values of Ri_c as $\mathrm{E} \rightarrow 0$. For $\sigma = 1$, the asymptotic value of Ri_c is close to 1, while for $\sigma = 2$ and 5, the asymptotic values are close

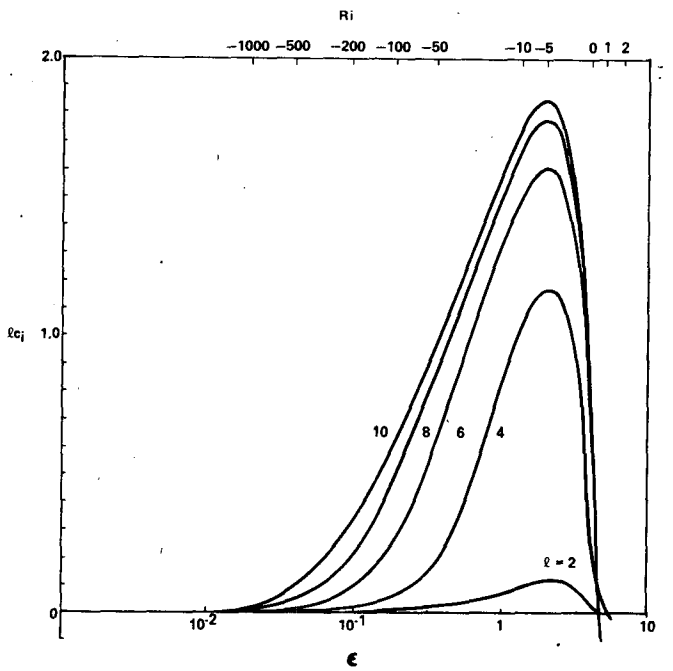

FIG. 8. Growth rates lc_i as a function of ϵ for different values of l and for $\sigma = 5$, $\Delta T = -4.5$ and $\mathrm{E} = 10^{-3}$. The upper abscissa shows the values of Ri corresponding to ϵ.

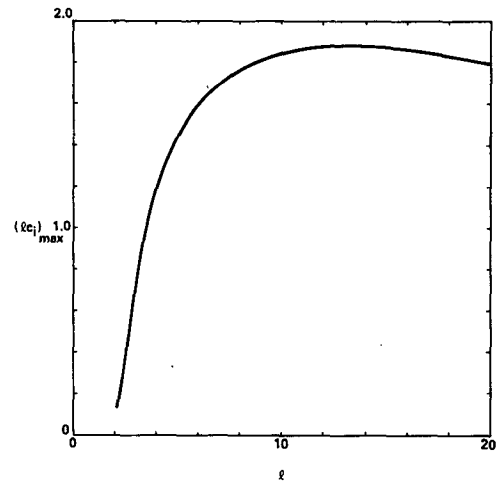

FIG. 9. The maximum growth rates as a function of l for the same conditions as Fig. 8.

to 1.075 and 1.695, respectively. The latter two values are significantly greater than 1. Thus, the trend for the asymptotic value of Ri_c is to increase with increasing σ for $\sigma > 1$. This fundamental dependence is in agreement with work of McIntyre (1970), although his model is somewhat different from the model being considered here (See Section 1). McIntyre found that the asymptotic value of Ri_c is given by

$$Ri_c = \frac{(1+\sigma)^2}{4\sigma}. \tag{16}$$

For σ = 1, 2 and 5, this relationship yields values of

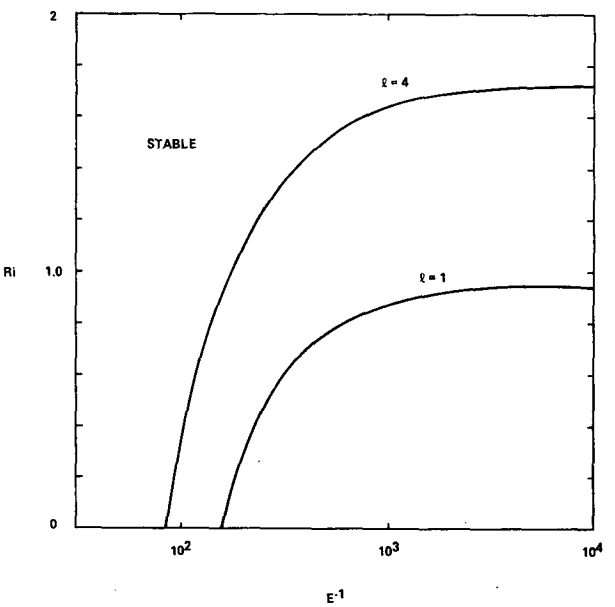

FIG. 10. Neutral stability curves as functions of E and Ri for different values of l and for σ = 5 and $\Delta T = -4.5$.

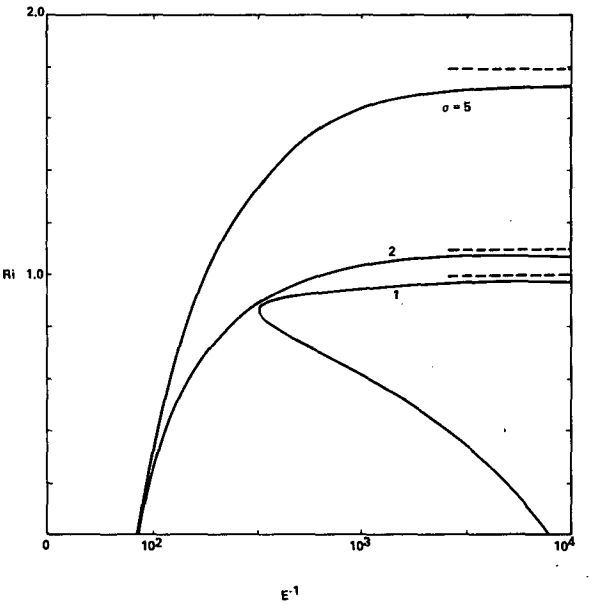

FIG. 11. Neutral stability curves as functions of E and Ri for different values of σ ($\geq$1) and for l = 4. The dashed lines are McIntyre's results.

Ri_c of 1, 1.125 and 1.8, respectively. These values are close to the values found from Fig. 11.

Fig. 11 also shows that as σ increases, the whole region of instability is markedly increased. The value of E_c increases drastically as σ is increased but there is no observable difference in the values of E_c for σ = 2 and 5.

Next, we present results for $\sigma < 1$. Again, the values for ΔT were chosen such that the range of Ri includes unity and values less than unity. Expression (15) indicates that when $\sigma < 1$ and $\Delta T < 0$, the maximum possible value for Ri is σ and thus the range does not include unity. However, when $\sigma < 1$ and $\Delta T > 0$, values of Ri can be obtained which are both greater and less than unity. We proceeded with $\Delta T > 0$.

Fig. 12 shows the neutral stability curves in the (E-Ri) plane for σ = 0.5 (ΔT = 0.2) and σ = 0.2 (ΔT = 0.5). The curves are for l = 12, the value which yielded the maximum value for Ri_c when all the other parameters were held fixed. Again, the values for Ri_c are seen to increase to specific asymptotic values as $E \rightarrow 0$. Note that the tendency to an asymptote is not as evident for σ = 0.5 as it is for σ = 0.2. The main features of Fig. 12 are the decrease in the value of Ri_c and the decrease in the total instability area as σ increases to unity. The results also indicate an increase in E_c with increasing σ.

Fig. 12 gives the values of Ri_c at $E = 10^{-4}$ for σ = 0.5 and 0.2 as 0.946 and 1.21, respectively. Fig. 13 is a comparison of all our results for the largest asymptotic ($E = 10^{-4}$) values of Ri_c with McIntyre's

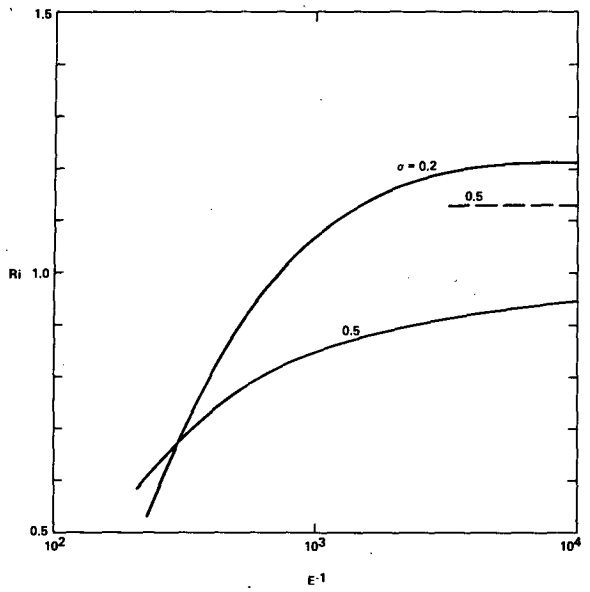

FIG. 12. Neutral stability curves as functions of E and Ri for different values of σ (<1) and for $l = 12$. The dashed line is McIntyre's result.

results as a function of σ. The dots are our results and the continuous curve is a plot of expression (16). Note that McIntyre's criterion yields a symmetric dependence of Ri_c as a function of σ about $\sigma = 1$. The results of the present study agree well with McIntyre for $\sigma \geq 1$ but give lower values for Ri_c for $\sigma < 1$.

5. Conclusions

The stability of a nonlinear rotating Hadley cell has been examined with respect to symmetric perturbations. This Hadley cell was derived previously (see I) and contains both Ekman and thermal boundary layers. The stability analysis is based on the Navier-Stokes equations and considers infinitesimal waves with vertical and meridional structure but no zonal structure. The stability analysis was performed numerically. For examining the parametric behavior of symmetric baroclinic instability, the work is an improvement over the previous work in which idealistic basic states were used, since a realistic one is now used and since the stability analysis includes both viscous and thermal diffusion effects.

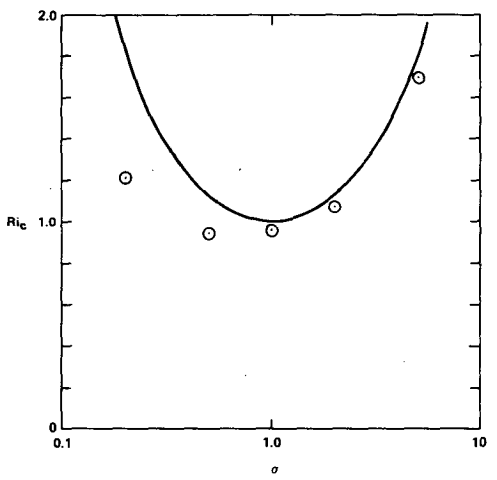

FIG. 13. A comparison between the critical value of the Richardson number Ri_c as calculated from Eq. (16) (curve) and the results presented in this paper as a function of σ for $E = 10^{-4}$ (circles).

The computations cover the following ranges of the non-dimensional parameters: $0.2 \leq \sigma \leq 5$, $10^{-2} \leq \epsilon \leq 10^2$, $10^{-4} \leq E \leq 10^{-1}$, $-4.5 \leq \Delta T \leq 0.5$, and $-100 \leq Ri \leq 2$. It was found that the instability sets in when Ri is close to unity and that the critical Richardson number Ri_c is a strong function of both σ and E for the cases considered. We extrapolated from these cases to obtain values of Ri_c for the inviscid limit $E \to 0$ and found that Ri_c has a maximum value close to unity for $\sigma = 1$. The general trend of these results is in agreement with McIntyre (1970) and for $\sigma \geq 1$ the agreement is very good but for $\sigma < 1$ it is not so good. We should not be surprised to find differences between the present and previous work because of the differences in the basic states and other aspects of the models.

We also found for fixed σ that Ri_c decreases with increasing E until a critical value of E is reached beyond which the fluid is stable. The principle of exchange of stability was not assumed and growth rates were calculated. A wavelength of maximum growth rate occurring for small wavelengths was found. For our model overstability was not found. Some computations were performed for $Ri < 0$. In particular, for $\sigma = 5$ the growth rate maximum occurs at about $Ri = -4$. No discontinuities in the growth rates are noticeable when Ri changes sign. This result indicates a smooth transition from symmetric baroclinic instability to a convective instability.

Acknowledgments. B.N.A. wishes to acknowledge receipt of Contract NAS8-33386 from NASA/Marshall Space Flight Center which he held during the performance of this investigation. This research was supported by the Global Weather Program of the NASA Office of Space and Terrestrial Applications.

APPENDIX

Corrections to I

Several printing errors have come to our attention since the publication of our paper I. The following corrections should be made in Eqs. (18)–(25):

Equation	Term	Correction
(18)	$2Dv$	$-2Dv$
(19)	$2iDw/k$	$-2iDw/k$
(20)	$-\sigma\mathrm{Ro}(v + wDT)$	$\sigma\mathrm{Ro}(v - wDT)$
(23)-(25)	$\mathrm{Ro}(kU - lV)$	$\mathrm{Ro}(kU + lV)$
(23)	$2i(kDv - lDu)$	$-2i(kDv - lDu)$
(24)	$2ikDw$	$-2ikDw$
(25)	$i[\omega \cdots$	$\sigma i[\omega \cdots$
(25)	$\sigma\mathrm{Ro}(v + wDT)$	$\sigma\mathrm{Ro}(v - wDT)$

REFERENCES

Antar, B. N., and W. W. Fowlis, 1981: Baroclinic instability of a rotating Hadley cell. *J. Atmos. Sci.*, **38,** 2130–2141.

Bennets, D. A., and B. J. Hoskins, 1979: Conditional symmetric instability a possible explanation for frontal rainbands. *Quart J. Roy. Meteor. Soc.*, **105,** 945–962.

Charney, J. G., 1947: The dynamics of long waves in a baroclinic westerly current. *J. Meteor.*, **4,** 135–162.

Eady, E. T., 1949: Long waves and cyclone waves. *Tellus*, **1,** 35–52.

Emanuel, K. A., 1979: Inertial instability and mesoscale convective systems. Part I: Linear theory of inertial instability in rotating viscous fluids. *J. Atmos. Sci.*, **36,** 2425–2449.

Hadlock, R. K., J. Y. Na and P. H. Stone, 1972: Direct thermal verification of symmetric baroclinic instability. *J. Atmos. Sci.*, **29,** 1391–1393.

Hathaway, D. H., P. A. Gilman and J. Toomre, 1979: Convective instability when the temperature gradient and rotating vector are oblique to gravity. I Fluids without diffusion. *Geophys. Astron. Fluid Dyn.*, **13,** 289–316.

——, —— and ——, 1980: Convective instability when the temperature gradient and rotation vector are oblique to gravity. II Real fluids with effects of diffusion. *Geophys. Astron. Fluid Dyn.*, **15,** 7–38.

Hide, R., and P. T. Mason, 1975: Sloping convection in a rotating fluid. *Advances in Physics*, Vol. 24, Academic Press, 47–100.

Kuo, H. L., 1956: Forced and free axially-symmetric convection produced by differential heating in a rotating fluid. *J. Meteor.*, **13,** 521–527.

McIntyre, M. E., 1970: Diffusive destabilization of the baroclinic circular vortex. *Geophys. Fluid Dyn.*, **1,** 19–57.

Quon, C., 1980: Quasi-steady symmetric regimes of a rotating annulus differentially heated on the horizontal boundaries. *J. Atmos. Sci.*, **37,** 2407–2423.

——, 1981: In search of symmetric baroclinic instability in an enclosed rotating fluid. *Geophys. Astron. Fluid Dyn.*, **17,** 171–197.

Solberg, H., 1936: *Le mouvement d'inertia de l'atmosphere stable et son role dans le theorie des cyclones.* Union Geodesique et Geophysique Internationale, VIieme Assemblée, Edinburgh, Vol. II, 66–82.

Stone, P. H., 1966: On non-geostrophic baroclinic stability. *J. Atmos. Sci.*, **23,** 390–400.

——, 1967: An application of baroclinic stability theory to the dynamics of the Jovian atmosphere. *J. Atmos. Sci.*, **24,** 642–652.

——, 1970: On non-geostrophic baroclinic stability: Part II. *J. Atmos. Sci.*, **27,** 721–726.

——, 1971: Baroclinic stability under non-hydrostatic conditions. *J. Fluid Mech.*, **45,** 659–671.

——, S. Hess, R. Hadlock and P. Ray, 1969: Preliminary results of experiments with symmetric baroclinic instability. *J. Atmos. Sci.*, **26,** 991–996.

Walton, I. C., 1975: The viscous nonlinear symmetric baroclinic instability of a zonal shear flow. *J. Fluid Mech.*, **68,** 757–768.

Weber, J. E., 1980: Symmetric instability of stratified geostrophic flow. *Tellus*, **32,** 176–185.